Reflection and Diffraction of Slow Electrons from Single Crystals of Tungsten

I. H. KHAN,* J. P. HOBSON, AND R. A. ARMSTRONG
Radio and Electrical Engineering Division, National Research Council, Ottawa, Canada
(Received 13 July 1962; revised manuscript received 5 November 1962)

Measurements have been made of the elastic reflection coefficient and total secondary electron coefficient for electrons with energies from 1–206 eV incident normally on single crystals of tungsten (112), (100), and (110). The apparatus permitted visual observation of the full diffraction pattern in the same energy range. Ultra-high vacuum techniques were used. The major features of the elastic reflection coefficient for incident energies below 20 eV were found experimentally to be associated with the specularly reflected or 0-0 diffraction beam. A model based on superposition of atomic scattering was found to give a better over-all description of the observations than a model based on a potential varying only along the normal to the crystal.

I. INTRODUCTION

EARLY measurements on the secondary emission of electrons from metals[1] under bombardment by primary electrons of energy less than 20 eV established two main results: (1) Maxima and minima were generally found in the secondary emission coefficient; (2) as the energy was lowered, the fraction of elastically reflected primaries in the secondary beam increased until it approached unity at a few electron volts.[2] The latter result has recently been confirmed in an ultra-high vacuum system.[3]

That the maxima and minima were related to the elastic component of reflected current was first demonstrated for polycrystalline cobalt.[4] The discovery of electron diffraction strongly suggested that the maxima and minima which had been observed, in the main, with polycrystalline targets were the result of diffraction effects, but experiments to correlate in detail the secondary emission coefficient with diffraction are rare and we know of only one[5] directed at this problem.

In this experiment, Farnsworth[5] measured the secondary emission coefficient and the diffracted beams in the same apparatus, while bombarding a single crystal of copper (100) at normal incidence. Two characteristic maxima were found in the secondary emission coefficient at 3- and 10.5-eV incident energy, respectively, as well as a series of lesser features at higher energies. While a reasonable correlation of these features with the diffraction beams was found, the experiment was not decisive. In particular, the observed set of 3-V beams did not appear in either principal azimuth and were not accurately reproducible. These considerations have led us to perform the measurements reported in this paper on single crystals of tungsten (112), (100), and (110) in which our objective has been similar to that of Farnsworth,[5] but with greater emphasis on the elastic component of the reflected beam. Our method was more closely allied with that of Ehrenberg,[6] using a fluorescent detector for the diffracted beams. The latter technique has received recent development by Scheibner, Germer, and Hartman.[7]

Tungsten was selected for the present study because its cleaning in an ultra-high vacuum system has been extensively investigated.[8] The choice of faces was based on the results of Smith,[9] who found the (112), (100), and (110) faces of tungsten to be the most stable.

There were several early secondary emission measurements on polycrystalline tungsten,[10] and there have been some more recent reflection measurements.[3,11] Reflection measurements with single crystals of tungsten have also been reported.[12] Low-energy diffraction measurements on tungsten (112) and (100) have been reported by Sproull,[13] and briefly by Germer *et al.*[14] These results are compared briefly with our own in Sec. V. Also in Sec. V, we compare our results with the predictions of alternative models of a crystal surface.

II. APPARATUS

A schematic diagram of the whole tube (Pyrex, Corning 7740) is shown in Fig. 1. An electron gun delivered a beam of electrons (1 to 206 eV) at normal incidence onto a single-crystal target of tungsten (112), (100), and (110). Diffracted beams at any angle passed

* Post-doctoral fellow.

[1] For bibliography see, K. G. McKay, *Advances in Electronics* (Academic Press Inc., New York, 1948), Vol. 1, p. 65.
[2] C. J. Davisson and C. F. Kunsman, Science **54**, 522 (1921).
[3] G. A. Harrower, Phys. Rev. **104**, 52 (1956).
[4] M. N. Davis, Nature **123**, 680 (1929).
[5] H. E. Farnsworth, Phys. Rev. **34**, 679 (1929).
[6] W. Ehrenberg, Phil. Mag. **18**, 878 (1934).
[7] E. J. Scheibner, L. H. Germer, and C. D. Hartman, Rev. Sci. Instr. **31**, 112 (1960).
[8] H. D. Hagstrum and C. D'Amico, J. Appl. Phys. **31**, 715 (1960).
[9] G. F. Smith, Phys. Rev. **94**, 295 (1954).
[10] A. H. Ahearn, Phys. Rev. **38**, 1858 (1931); H. E. Farnsworth, *ibid.* **25**, 41 (1925); O. Stuhlmann, Science **56**, 344 (1922); R. L. Petry, Phys. Rev. **28**, 362 (1926); H. E. Kreft, *ibid.* **31**, 199 (1928); V. I. Kasatochkin, Actaphysicochim. U.S.S.R. **2**, 317 (1935); E. A. Coomes, Phys. Rev. **55**, 519 (1939); K. G. McKay, *ibid.* **61**, 708 (1942).
[11] H. P. Meyers, Proc. Roy. Soc. (London) **A215**, 329 (1952); G. A. Harrower, Phys. Rev. **102**, 340, 1288 (1956); N. D. Morgulis and D. A. Gorodetskii, Soviet Phys.—JETP **3**, 535 (1956); D. A. Gorodetskii, Bull. Acad. Sci. U.S.S.R. **20**, 925 (1956); J. M. Bronshtein, *ibid.* **22**, 442 (1958).
[12] W. Boas and E. Rupp, Ann. Physik **7**, 983 (1930); E. Rupp and R. V. Meibom, *ibid.* **18**, 107 (1933); D. A. Gorodetskii, Soviet Phys.—JETP **34**, 4 (1958); P. Kisliuk, Phys. Rev. **122**, 405 (1961).
[13] W. T. Sproull, Phys. Rev. **43**, 516 (1933).
[14] L. H. Germer, E. J. Scheibner, and C. D. Hartman, Phil. Mag. **5**, 222 (1960).

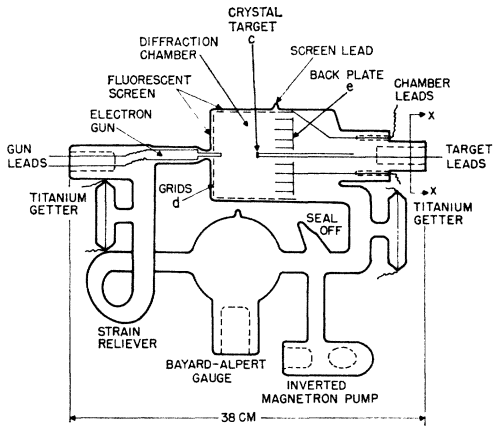

FIG. 1. Apparatus.

back through the diffraction chamber, penetrated a pair of nesting grids *d* (tungsten mesh), and were accelerated through 1000 V to the willemite fluorescent screen, where these beams could be viewed as spots. All diffraction angles could be observed except those obscured by constructional features. The back plate *e* collected any electrons missing the target, and was designed with cylindrical fins of tungsten to reduce reflection of electrons. The diffraction chamber, gun, and target assembly were cylindrically symmetric about the central axis. Reflection and secondary emission measurements were performed with fluorescent screen and grids *d* connected electrically, thus providing a cylindrical collector for electrons issuing from the target. Targets were replaced by cutting the tube at *X*–*X* in Fig. 1.

The remaining elements of the sealed-off tube measured or pumped the residual gases. The vacuum techniques used were those employed routinely in this laboratory.[15] After seal off, pumping was done with the titanium getters and the inverted-magnetron pump[16] which was incorporated into the system to pump the inert gases (mainly, helium and argon). With this pump operating, a base pressure of 10^{-10} Torr was achieved. The magnet (approximately 2000 G) necessary for this pump was removed manually just prior to measurements.

The tube was mounted inside Helmholtz coils which reduced the residual steady magnetic field to less than 2.5 mOe. Ac magnetic fields were less than 2.0 mOe. All tube parts were nonmagnetic. Magnetic fields, including that of the gun filament, played no measurable part in the measurements.

The crystals were supported by a sleeve of tungsten foil (0.001 in.) and were outgassed by electron bombardment from an internal heater until they could be raised to 2200°K at a total pressure less than 2×10^{-10} Torr for 15 sec. 2200°K is the temperature quoted by Hagstrum and D'Amico[8] for cleaning tungsten. In this method of heating no electrons struck the crystal face during outgassing. The adsorption of the residual active gas on the target face after flashing could be monitored directly by the shift in contact potential of the target as measured by a retarding field plot on the electron beam (see Sec. III). No shift was observed during the first two hours after flashing, during which time any particular run could be completed. Other evidence suggested a monolayer time for active gas of the order of 20 h. Thus, the results are considered representative of a clean surface.

The crystals were cut from a single crystal of tungsten about 4 mm in diameter and 4.5 cm long with the [111] direction approximately along the axis. Spectrographic analysis of a sample of the crystal in a dc arc with a 3.4-m Ebert spectrograph showed 1–5 ppm Cu, 1–10 ppm Fe, less than 1 ppm Mg. Cutting was done with a rubber-bonded carborundum wheel 1.5 in. in diameter and 0.015 in. thick, rotating at approximately 3600 rpm. Subsequent etching in normal KOH with the crystal as the anode at 0.5 A dc for 15 to 60 min produced a surface suitable for x-ray analysis. Excellent back reflection patterns were obtained. Cutting accuracy was $\pm1°$. The crystals were next ground on emery paper of increasingly finer grade, with alcohol as the lubricant, followed by polishing with alumina type *A* on microcloth in water, and then with alumina type *B* on kitten-ear cloth in water. Following this, the crystals were electropolished under the following typical conditions: crystal as anode in 0.375*N* NaOH at a voltage of 6.3 V dc with a current of 13 mA, anode to cathode spacing 6 mm, for 15 min. The resulting surfaces gave good electron diffraction patterns with Kikuchi lines, and appeared smooth as judged with carbon-replica techniques in the electron microscope, down to distances at least as small as 30 Å, the limit of the technique used. After electropolishing, the tungsten (110) crystal was heated to 2200°K for 2 h at a pressure below 2×10^{-10} Torr, these conditions being representative of those to be expected later in the low-energy reflection/diffraction tube, to establish whether this heat treatment caused any change in the electron diffraction and microscope results. None was found at this time.

A schematic diagram of the electron gun is shown in Fig. 2. The tungsten filament source was 0.005-in. wire coiled to a diameter of 1 mm with one lead returning down the center of the coil. Electrodes 1 and 2 constituted an emission system, 3 and 4 a univoltage electrostatic lens, 5 and 6 two pairs of deflection plates, each being curved and occupying almost a quadrant to conform to the general gun geometry. The tube *a* served as collimator. A final electrode, *b*, operated at the potential of the diffraction chamber, shielded the chamber from the collimator potential but performed three other important functions. With *b* lower in potential than the collimator, an electrostatic focusing lens was formed at the gun output which greatly assisted in focusing the

[15] P. A. Redhead, E. V. Kornelsen, and J. P. Hobson, Can, J. Phys. **40**, 1814 (1962).

[16] E. V. Kornelsen, in *Transactions of the Seventh National Symposium on Vacuum Technology, 1960* (Pergamon Press, New York, 1961), p. 29.

beam onto the target at low energies. A lens at this point has also been found useful by Farnsworth.[17] Electrode b also prevented secondary electrons from the collimator entering the diffraction chamber. Further, current measurements on b assisted in the interpretation of the angular dependence of the reflection results. Empirically it was found possible to deliver onto the target 10^{-6} A at an energy of 10 eV, and 10^{-7} A at energies between 3 and 10 eV, while confining 90% or more of the beam onto the target. At 1 eV it was possible to deliver 10^{-7} A confining 75% to the target. For the diffraction measurements more current was desirable and less definition was permissible, and for these measurements beam currents between 10^{-6} and 10^{-5} A were normally used. Focusing was not a serious problem above 10 eV. A typical set of operating voltages was: $V_1=0$, $V_2=150$, $V_3=15$, $V_4=190$, $V_{5(\text{mean})}=85$, $V_{6(\text{mean})}=85$, $V_a/V_b=2.4$. The deflection voltages on V_5 and V_6 were quite critical but always less than 3 V. The delivery point of the gun was brought out beyond the grids d to ensure the electrons reaching the screen near the gun had interacted with the target first. The glass envelope in this region was necked down to reduce the blind angle for electrons returning from the target toward the gun. The blind colatitude angle was 2.5° (colatitude angle θ is the angle between the normal to the target face and the direction of the reflected electrons). The fluorescent screen of willemite was laid down on a conducting coating of SnO on the glass. The corner of the tube produced other blind colatitude angles for $38.1°\leq\theta\leq42.5°$. Observations at certain azimuth angles ϕ were also obscured by axial supports, but these were sufficiently thin (≤2 mm) that spots in the vicinity could generally be detected. Early in the experiment a short developed between the grids d, but since this did not affect the main purposes of the experiment, the grids were used as one, and colatitude angles were calculated on the assumption that electrons followed straight-line paths from the target to the outer grid and were there accelerated in a straight line normal to the screen.

III. EXPERIMENTAL PROCEDURE

The central problem in the measurements at low energies was that of delivering a beam of adequate intensity onto the target face. The experimental criterion used throughout the measurements for checking this was the minimization of the ratio I_e/I_c; that is, the currents to the back plate and the target, respectively. This focus condition was repeatedly checked. The target mount was constructed in all cases so that the polished area of the crystal represented more than 90% of the total area of the target electrode "seen" by the incident beam. It was not to be expected that the ratio I_e/I_c could be reduced to zero since some electrons reflected by the target would be reflected again by the grids d and

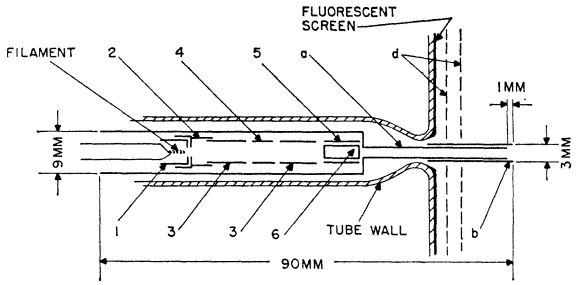

FIG. 2. Electron gun.

be measured finally as a current on e. The number of these multiply reflected electrons returning to the target was small, from solid-angle considerations. A check on the degree of primary beam focusing could be made by calculating R (or δ) in two ways and comparing the results:

$$R=\frac{I_b+I_d}{I_b+I_d+I_c}, \tag{1}$$

or

$$R'=\frac{I_b+I_d+I_e}{I_b+I_d+I_c+I_e}. \tag{2}$$

If the entire primary beam strikes the target (a condition generally valid above 10 eV), then R' is the better measure; whereas if a portion misses the target, R is a better measure, and so is more reliable at low energies. It was found experimentally that R and R' did not differ by more than 10% above 3 eV. Thus, in the results given in Sec. IV, R (and δ calculated in the same way) has been used as a valid measure over the whole experimental range. Below 1 eV a value of $I_e/I_c<0.3$ could not be achieved, and 1 eV has been arbitrarily designated as the lower limit of reliable measurement.

The zero of impact kinetic energy of the electrons on the target was established by retarding field measurements. The emitting portion of the filament was operated about 4 V above ground and all the chamber voltages were set to 6 V, i.e., the kinetic energy of electrons in the chamber was about 2 eV. Careful gun focusing was carried out and the current to each chamber electrode was measured while its voltage was varied, all other chamber voltages being held at 6 V. Typical results are shown in Fig. 3. Here electrode d represents the two grids and fluorescent screen joined together. The break points were taken in the usual way, as representing the voltage at which the slowest electrons in the beam were turned back at their respective electrodes. It was checked that setting all chamber voltages at 10 V rather than 6 V during the retarding-field measurements caused no change in the location of the break points, indicating that they were true measures of a surface property rather than some electron-optical parameter. The absolute error in this method of measuring the kinetic energy of impact of the electrons

[17] H. E. Farnsworth, Phys. Rev. 31, 405 (1928).

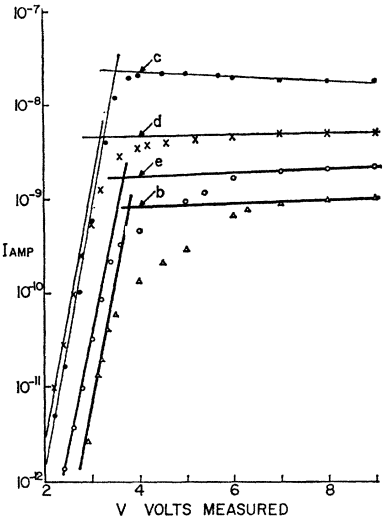

FIG. 3. Retarding field plots.

on the target is estimated at ± 0.5 eV. All voltages and energies quoted below have been corrected assuming the break points as zero for the respective electrodes. The break-point measurements were fully reproducible over the course of the experiments.

The measurements of R, the coefficient of elastic reflection were taken with $V_b = V_d = V_e = 1$ V, while V_c was varied from 1 to 206 eV. I_b, I_c, I_d, and I_e were measured for all values of V_c and R was calculated from Eq. (1). In a single run all focusing was done at the beginning, while during the run only V_c was changed. Hemispherical retarding geometry would have been preferable, but the results of Fig. 3 suggest that cylindrical geometry should not introduce serious error.

With chamber voltages set as for R, measurements were made of I_b, the current to electrode b, and the ratio I_b/I_t calculated, where I_t was the total current entering the diffraction chamber ($I_t = I_b + I_c + I_d + I_e$). I_t was chosen as the normalizing quantity for experimental convenience, because the variation of I_b as a function of V_c could be quickly measured, I_t remaining fixed, without the necessity of measuring all four currents. The ratio provided a measure of current concentrated in the specular direction (or in the 0-0 diffraction beam).

The measurements of δ, the coefficient of total secondary emission were taken with $V_b = V_c = V_d = V_e$ which were varied from 1 to 206 eV. The field conditions at gun output were continuously varying and the potential on collimator a was adjusted to maintain proper focus.

Primary beam currents varying over a factor of 50 were used during the measurements with no change in the results.

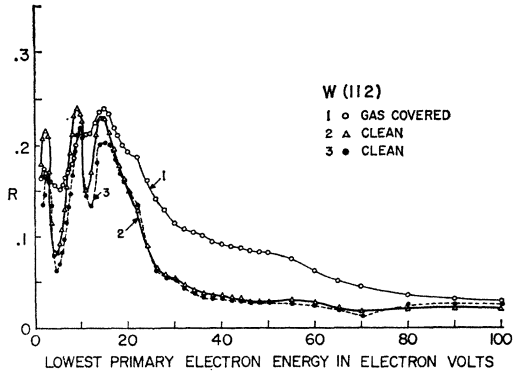

FIG. 4. Elastic reflection coefficient R for tungsten (112).

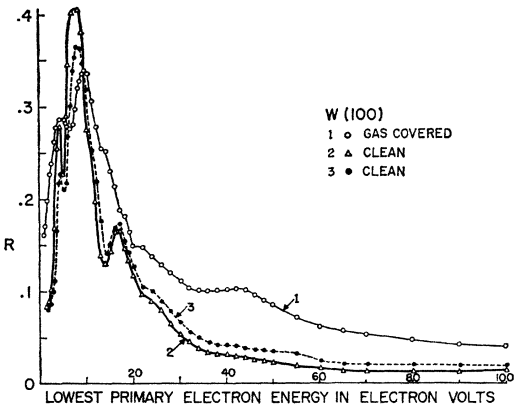

FIG. 5. Elastic reflection coefficient R for tungsten (100).

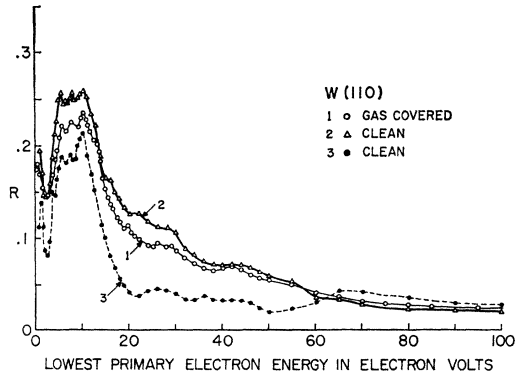

FIG. 6. Elastic reflection coefficient R for tungsten (110).

The diffraction data were taken with a voltage ratio between grid and target of $V_d/V_c = 0.7$, a condition which produced sharp spot definition without a serious shift in spot location. Photographs of the front face of the tube were taken in a mirror outside the tube, but a wider range of colatitude angles could be studied by additional measurements of spot locations on the tube sides.

IV. RESULTS

1. Measurements of R, δ, I_b/I_t

The results of the measurements of R and δ are given in Figs. 4–9 for the three crystal faces. Figure 10 gives

I_b/I_t for $W(112)$. The results of I_b/I_t for the other crystals were similar and have been omitted for brevity. Data were also taken in the 100–206 eV range but showed no major features and have been omitted for the sake of expanding the low-energy scales.

The curves labelled 1 were taken after the crystals had been outgassed at 2200°K for about 1 h and then allowed to adsorb the residual gases of the tube for several days at room temperature. The identity of the residual active gas was not measured and is not known. However, similar vacuum systems gave a mixture of CO and H_2 as the residual active gas. Before curves 2

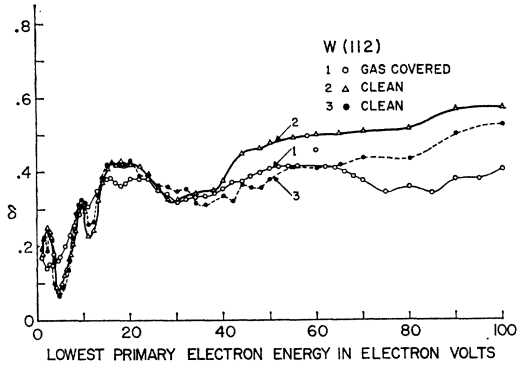

FIG. 7. Total secondary emission coefficient δ for tungsten (112).

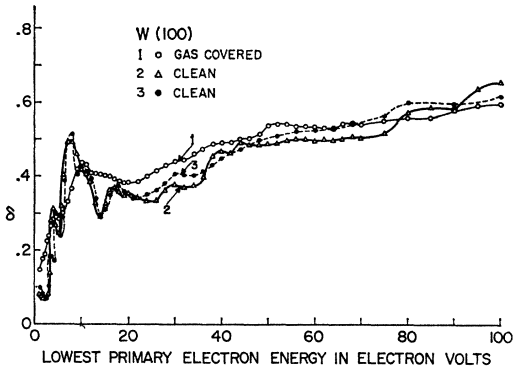

FIG. 8. Total secondary emission coefficient δ for tungsten (100).

were taken the target was further outgassed for 1 to 3 h at 2200°K, followed by a series of flashings until clean surface conditions were achieved. Between curves 2 and 3 another outgassing period of 1 to 2 h at 2200°K, followed by flashings, occurred. The purpose of this third outgassing was to establish whether the heat treatment was causing any progressive change in the results. In general, as may be seen from Figs. 4–10, the answer was negative and curves 2 and 3 are considered representative of clean surfaces.

The value of R at a fixed electron energy was found to be a function of the target temperature but the effect was not large enough to alter the results of Figs. 4–6,

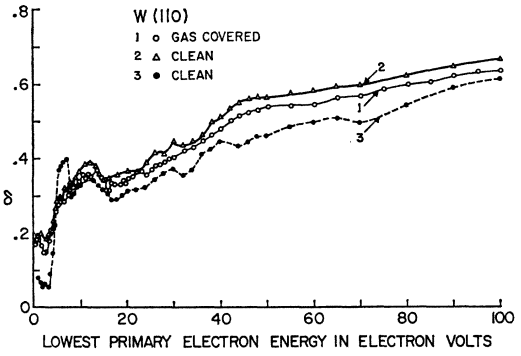

FIG. 9. Total secondary emission coefficient δ for tungsten (110).

which are representative of the target at room temperature.

The following conclusions, of which the first three are considered additive to existing knowledge, were drawn from a study of the curves:

(1) The envelope of the elastic reflection coefficient R for all faces has a value 0.07 to 0.2 near zero energy, rises to a maximum value 0.2 to 0.4 in the energy range below 20 eV, and falls away quite rapidly to values <0.04 as the energy increases to 100 eV.

(2) The dominant characteristics of all the curves of Figs. 4–10 in the range 1 to 20 eV are associated with the 0-0 diffraction beam.

This conclusion rests on the numerical values and form of the currents measured on electrode b and on visual evidence previously reported for the (110) face,[18] which was subsequently confirmed for all faces. Electrode b presented a solid angle of 0.0015 solid radian to an electron reflected from the center of the target. For a cosine distribution of reflected electrons the expected fraction intercepted by b would have been 0.0005. However, as may be seen in Fig. 10, values 100 to 1000 times this were found, indicating strong peaking of intensity in

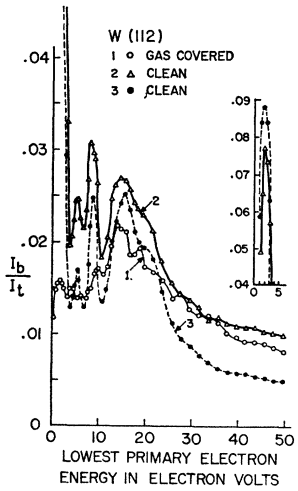

FIG. 10. I_b/I_t for tungsten (112).

[18] J. P. Hobson and I. H. Khan, Phys. Rev. 123, 1242 (1961).

the backward direction. All the curves for I_b/I_t had the same form as the corresponding R, reproducing many of the same fine structure details in somewhat distorted form. The actual fraction intercepted by b might be expected to depend on the details of gun focusing and alignment. This result was confirmed experimentally by varying gun focusing and beam deflection, and the effect can account for the variations observed in the absolute value of I_b/I_t. The visual evidence mentioned above consisted of the result that the only diffraction beam visible for each crystal below 12–20 eV was seen close to the neck of the tube in Fig. 2 in the location expected for the 0-0 diffraction beam. Photographs of this spot were of poor quality because of background light from the gun filament.

The property of the I_b/I_t curves previously described,[18] that the relative amplitude but not the location of the structural features depended upon the chamber focusing conditions, was rechecked for each crystal.

(3) The curves for R show pronounced and reproducible fine structure for the clean surfaces for energies below 20 eV, this fine structure differing for each face.

(4) An elementary diffracting unit had a linear dimension of at least 20 atoms.

The numerical value of I_b/I_t for the peak at 2.5 V in Fig. 10 is about $\frac{1}{2}$ the corresponding value of R. Since electrode b subtended a linear angle of 5° at the target this gives the approximate half-width of the 0-0 diffraction beam as about $\delta\theta=5°$. From the relation $\delta\theta=\lambda/Nd$, where N is the number of atoms in the diffracting unit, λ is the electron wavelength, and d is the atomic spacing in the surface grating, we find that $N\doteqdot 20$. Since the beam spread may be caused by factors other than the number of atoms in the diffracting unit this represents a lower bound on the linear dimension of the diffracting unit. Similar results were obtained for the other faces.

(5) All the curves for δ have the same general shape, increasing from a value about 0.07 to 0.2 near zero energy to a plateau or shallow maximum in the range of energies below 20 eV, thereafter continuing a general upward trend to a value about 0.4 to 0.6 at 100 eV.

(6) Many of the fine structure details seen in the corresponding R curve are found also in the δ curve, but in subdued form.

(7) The magnitudes of R and δ remain the same up to an energy between 5 and 10 eV, giving an energy in this range as the threshold for secondary emission. However, the curves are of such complexity in this range that more detailed conclusions appear unreliable.

(8) The trend of the results for the gas-covered surfaces are similar to those for the clean surfaces, but the latter have the fine structure details more fully developed.

(9) There is little decisive structure in R or δ at energies above 20 eV in the range where it is known from the diffraction data described below that diffraction beams are continually passing through maxima.

(10) While generally curves 2 and 3 for R and δ are reproducible there are some exceptions, particularly tungsten (100), $R2$, and 3. Since the gun collimator a presented a solid angle to electrons returning from the target comparable in size with that presented by b, some variations in R and/or δ might be expected as a result of reflected electrons escaping into the gun. Over this source of error there was no systematic control except that the gun focusing conditions, once set, were altered as little as possible during a run. The magnitude of the error was related to the magnitude of I_b/I_t, and in the special case mentioned above where there was a decisive fall between runs 2 and 3 for R, there was also a decisive increase in I_b/I_t. For these reasons it appears advisable to consider in interpretation only those features of Figs. 4–10 that are decisively reproduced.

Before an attempt is made to interpret results 1–3 above, it is important to examine the diffraction data obtained in order to establish as clearly as possible the crystalline state of the surface being bombarded.

2. Diffraction Results

These diffraction results refer to all diffraction data exclusive of the 0-0 diffraction beam. The central purpose of this data, which was all obtained from the fluorescent screen, was to establish whether the crystals being bombarded were indeed single in the surface layers and whether there was any evidence of surface structure unlike that of the underlying crystal. Spot patterns of which Fig. 11 is an example were studied for all crystals between 1 and 206 eV.

The diffraction patterns from tungsten (112) were studied in particular detail because this face was studied previously by Sproull,[13] who found a system of diffraction maxima which did not fit the general theory for low-energy electron diffraction as outlined by Davisson and Germer.[19] Farnsworth[20] and Thomson[21] independently suggested that surface etching was responsible for Sproull's anomalous results, but to our knowledge no experimental repetition of Sproull's measurements had been made to check this point. (We are indebted to H. E. Farnsworth for directing our attention to these two Letters.) The theory for the (112) face of tungsten has been explicitly given by Sproull[13] and we do not repeat it here, but use Sproull's nomenclature. Figure 12 shows our experimental results in the azimuth $\phi=0$, i.e., in a direction at right angles to the rows of largest atomic spacing in the (112) face. The observed diffraction maxima, marked as spots, have been assigned a visual intensity. The lines designated by n_1 are the orders of the surface grating and the lines designated by n_2 are the orders of the volume grating. No correction for inner potential has been made. The shaded regions in

[19] C. J. Davisson and L. H. Germer, Phys. Rev. **30**, 705 (1927).
[20] H. E. Farnsworth, Phys. Rev. **44**, 417 (1933).
[21] G. P. Thomson, Phys. Rev. **44**, 417 (1933).

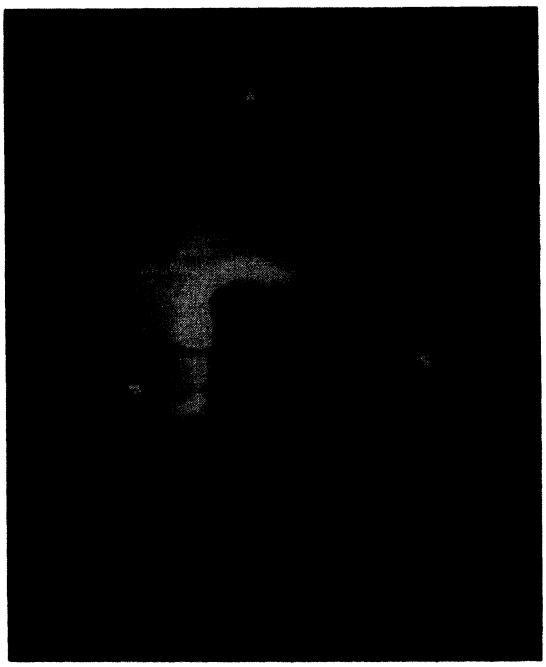

FIG. 11. Photograph of front face of tube in mirror showing diffraction pattern from tungsten (112) at 56 eV. Upper spot is 10 reflection ($\phi=90°$); side spots are 01 reflection ($\phi=0°$) and $0\bar{1}$ reflection ($\phi=180°$).

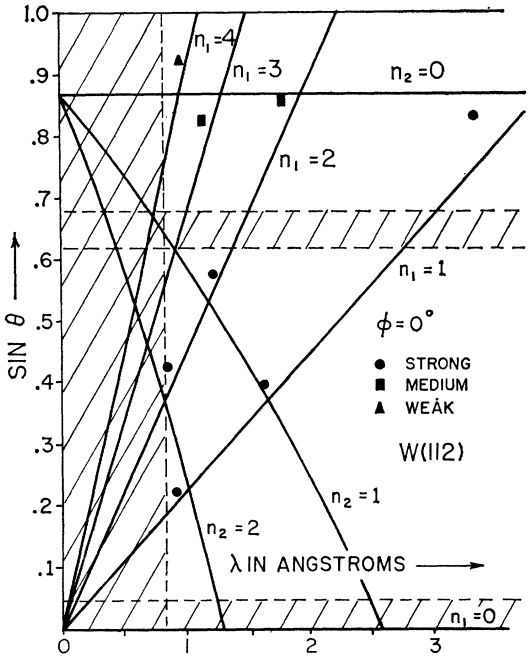

FIG. 12. Comparison of diffraction theory and experiment for tungsten (112); $\phi=0$.

Fig. 12 represent values of the parameters which could not be realized experimentally. A diffraction maximum is predicted by the model at every intersection of lines. It may be seen that all predicted maxima in this azimuth were found within the experimental error, with the exception of $n_1=3$, $n_2=1$, which was sufficiently close to a shaded area to escape detection. Results for all azimuthal angles were similar to the results of Fig. 12 and are summarized in Table I for incident energies from 1 to 206 eV for $W(112)$.

The central conclusion from Table I is that the clean (112) crystal was single up to the surface and no unexpected surface structures were observed. Even when a monolayer of ambient active gas was present on the surface the principal effect on the diffraction patterns was the same as that found in the reflection measurements, namely, one of diminishing the intensity of diffraction effects. Since no results similar to Sproull's[13] were found, we must support Farnsworth's and Thomson's explanation of Sproull's results. However, a number of maxima were predicted which were not found. Some could be assigned to experimental blind angles, but most could not. Of the latter, all had predicted $\theta\geq 60°$ and also satisfied a condition which has been called the "collision angle condition" in Table

TABLE I. Comparison between theory and experiment for tungsten (112).

Clean		Gas covered	
No. of maxima predicted by model	81	No. of clean surface maxima eliminated by gas adsorption	10
No. of observed maxima	25 strong, all predicted; 12 medium, all predicted 16 weak, all but 3 predicted (1 assignment doubtful); 7 very weak, all but 1 predicted (2 assignments doubtful)	No. of clean surface maxima reduced in intensity by gas adsorption	23
		No. of clean surface maxima unchanged by gas adsorption	27
		No. of new maxima apparently produced by gas adsorption	3 (all in positions predicted by model)
No. predicted by model but not observed	25		
No. predicted by model but probably ruled out by experimental obstructions	7		
No. predicted by model and not observed for which the collision angle condition is satisfied	18 (all θ's $\geq 60°$)		

I. This means that the direction of exit from the crystal of the diffraction maximum in question intersected a row of atoms in both the second and first layers. This has been termed the collision angle condition even though the atoms of the second and first layers do not lie in the same plane. Actually, this collision angle conclusion is a weak one, because it is fairly easy to satisfy the collision angle condition at wide colatitude angles.

The diffraction data for the (100) face were obtained only from photographs of the front face of the tube. The range of the data was thus smaller than for tungsten (112). Complete agreement with the theory was found over the measured range, and it was concluded that the crystal surface was undisturbed by the heat treatment. Adsorbed gas once again diminished the intensity of diffraction effects but gave no new surface structures.

The (110) crystal was installed in the apparatus twice. On the first occasion the outgasser failed before decisive clean surface conditions were achieved, but the diffraction patterns gave full agreement with the theory over the whole observation range of the apparatus. Measurements of R, I_b/I_t, and δ were taken. On the second occasion clean surface conditions were achieved but diffraction patterns taken between runs 2 and 3 of Figs. 6 and 9 were clearly indicative of surface recrystallization, the patterns having many of the directional properties of the (110) face, but indicating spacing between rows of scattering atoms many times the basic spacing of the tungsten (110) face. Measurements of R, I_b/I_t, and δ, however, differed only in minor details from measurements made on the first occasion. Unfortunately, we cannot pinpoint exactly when the surface change took place. Thus, the measurements of R and δ for this crystal are less suitable for theoretical interpretation than those for tungsten (112) and (100). As with the other crystals, adsorbed gas played a second order role in the results.

Normally, the angular half-width of a diffraction spot at 200 V was about 1° as judged visually. This gives a minimum size of an elementary diffracting unit at least 20 atoms in linear dimension, a result in agreement with a similar deduction made from the 0-0 diffraction beam in Sec. IV.1.

V. DISCUSSION OF REFLECTION RESULTS

1. Comparison with Previous Results on W

The majority of the previous work on tungsten (see Sec. I) used polycrystalline targets. It is difficult to make detailed comparisons between this work and the present results. However, if it is assumed that the data from a polycrystalline target under varying conditions of cleanliness will be some composite of the type of data presented in Figs. 4–9, then the composite results would differ essentially from the curves of Figs. 4–9 only in the fine structure details, since most other features are similar for the three faces. This is just the result that has been obtained for most polycrystalline samples, with respect to the general shape of the curves, the approximate magnitudes involved, and the general relationship between elastically reflected primaries and true secondary electrons.

For single-crystal targets the comparison can be more specific. Already discussed (see Sec. IV) has been the comparison between Sproull's diffraction results and the present ones for the (112) face. For the (100) face the present results are in essential agreement with those of Sproull, but provide data at lower incident energies. The structure observed by Kisliuk[12] in the reflection coefficient from tungsten (310,831) are similar in general appearance to the present R curves. Interpretation of Kisliuk's data, however, is complicated by the presence of a large magnetic field which converts all directional properties into the normal direction.

Measurements of R and δ by Gorodetskii[12] are comparable with the present results obtained for a gas-covered surface. Our conclusion from Table I of Sec. IV that the adsorption of ambient gas on tungsten gives minor changes in the diffraction pattern is in accord with a comment by Germer, Scheibner, and Hartman.[14]

Low-energy electron diffraction is being increasingly applied to the analysis of surface structures of adsorbed atoms on single crystals.[22,23] The results presented here show that adsorbed atoms do not always give first-order effects and, hence, the technique is probably limited to specific adsorbate-adsorbent combinations.

2. Comparison with Predictions of Theoretical Models

The diffraction results in this experiment demonstrated that the crystals used were ideal to first order. This suggests that the theory for the reflection coefficient be treated in two parts: first, for an ideal crystal, and second, as modified by surface imperfections.

Steps in the surface between relatively large ideal areas of the crystal will produce first-order effects in the reflection coefficient if the coherence width of the beam is sufficiently large. Such steps will generate additional minima in the reflection coefficient at those energies at which destructive interference between reflections from the different areas occurs. Herring[24] has given a theory for facet growth in tungsten, which provided a remarkable fit to the observations of Smith[9] on tungsten wires. Smith found that (112), (100), and (110) faces were preferentially developed. If this theory is applied for the heat treatments used in the present experiments, facets at least 1000 atoms in diameter result. While the validity of Herring's theory for a flat surface rather than a wire is not certain, the theory does suggest that surface steps

[22] J. J. Lander and J. Morrison, J. Chem. Phys. **37**, 729 (1962).
[23] L. H. Germer, A. U. MacRae, and C. D. Hartman, J. Appl. Phys. **32**, 2432 (1961).
[24] C. Herring, *Structure and Properties of Solid Surfaces* (University of Chicago Press, Chicago, Illinois, 1953), p. 5.

play no role in the observations reported here. This conclusion is supported by the reproducibility of the results after heat treatment of the crystals.

As mentioned in Sec. IV, the angular width of the diffracted beams gave an average area of ideal surface at least 20 atoms in diameter. The experiment provides a lower bound on the diameter of coherence of the electrons in the beam from the following argument. At 1 eV only 75% of the beam could be held on the crystal face. There was, thus, uncertainty in the ratio of the momentum component in the plane of the crystal (Δp_y) to the momentum toward the crystal (p_z) equal to the angle subtended by the crystal at the gun output.

$$\Delta p_y/p_z \doteq \tfrac{1}{10}. \quad (6)$$

This equation may be solved for Δp_y and the result substituted into the uncertainty relation $\Delta p_y \Delta y \geq \hbar$ to give $\Delta y \geq 7$ atomic spacings. This means that at 1 eV the beam is coherent at least over an area with a diameter of 7 atoms. Thus, the limitation of beam coherence can account for the size of the elementary diffracting unit and it is necessary to establish whether reflection from an ideal crystal can account for the observations of the reflection coefficient. In Secs. *V.2a* and *V.2b* two alternative models of an ideal crystal surface are examined.

2.a One-Dimensional Models of a Crystal Surface

One of our main conclusions in Sec. IV was that the major features of the reflection of slow electrons occurred along the normal to the crystal surface. The theory of thermionic emission[25] and, in particular, that of the periodic deviations from the Schottky effect[26,27] have successfully used a one-dimensional potential variation along the normal to the surface. The latter studies provide a calculation of R for electrons impinging at normal incidence at $E=0$. Using a constant inner potential of 10 eV for tungsten, joined to a classical image potential at the surface of the metal, Juenker *et al.*[26] obtained $R\sim 0.04$ at $E=0$. With the same inner potential but with an image potential modified to account for exchange and correlation, Cutler and Gibbons[27] found $R=0.36$ for $E=0$ and obtained excellent agreement between theory and experiments for the periodic deviations in the Schottky effect. These results are in the same range as the results reported here.

MacColl[28] joined a one-dimensional sine-wave potential to the image potential and found diffraction bands or narrow ranges of E in which R rises sharply to unity. Parameters appropriate to tungsten have been inserted into MacColl's calculation and the expected result plotted in Fig. 13. The locations of the diffraction

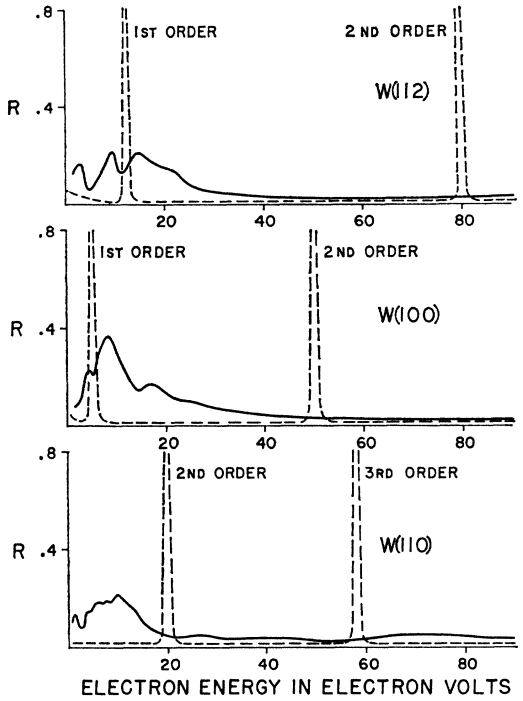

FIG. 13. Elastic reflection coefficient vs energy of electrons incident normally on single crystals of tungsten. Solid lines: experiment; dashed lines: theory based on MacColl's calculations with $V_0=10$ eV.

maxima correspond to the intersections of the curved lines of Fig. 12 with the λ axis after suitable modification for the inner potential. The bands in Fig. 13 do not occur at the same energy as the major maxima observed and they are narrower in energy. Herring and Nichols[25] point out that inelastic processes will cause R to be less than unity. Inelastic effects progressively reduce the calculated R with increasing energy. The measured R shows additional fine structure not predicted by MacColl's theory. Steps on the surface could cause additional minima in the theoretical R at approximate energies which might provide a better match to the experimental fine structure. However, no one-dimensional model generates the over-all shape of the R curve [result (1) of Sec. IV.1] and for this reason we have examined an alternative model for the crystal surface, the outlines of which are described by Juretschke.[29]

2.b Atomic Model of a Crystal Surface

The exact form of the potential near the nucleus is very important in low-energy electron scattering. To demonstrate this sensitivity, the elastic scattering from the free tungsten atom was calculated. The Fermi-Thomas potential was calculated by the procedure described by Schiff,[30] together with the screening factors of Bush and Caldwell.[31] The procedure described by

[25] C. Herring and M. H. Nichols, Rev. Mod. Phys. **21**, 185 (1949).
[26] D. W. Juenker, G. S. Colladay, and E. A. Coomes, Phys. Rev. **90**, 772 (1953).
[27] P. H. Cutler and J. J. Gibbons, Phys. Rev. **111**, 394 (1958).
[28] L. A. MacColl, Bell System Tech. J. **30**, 888 (1951).
[29] H. J. Juretschke, *The Surface Chemistry of Metals and Semiconductors* (John Wiley & Sons, New York, 1952), p. 38.

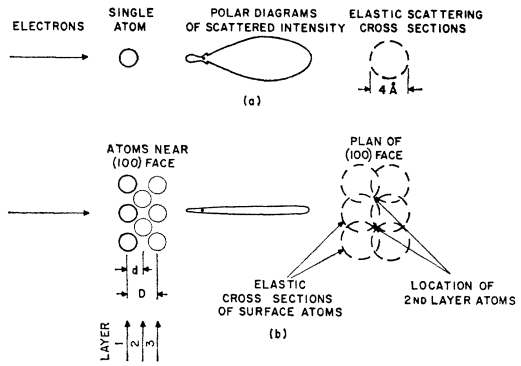

FIG. 14. Illustration of angular dependence and elastic cross sections for scattering of electrons from (a) single atoms, and (b) a two-dimensional array of atoms. Numerical values used are those for mercury atoms at 20-eV incident electron energy.

Massey and Burhop[32] for the elastic scattering of electrons by this potential was applied. It was found that more than 90% of the contributions to the phase-shift integrals occurred within a radius of 1 Å of the center of the atom. This is the region in which the atomic potential is nearly unaffected when the atoms are assembled into a solid.

Here we examine a model in which the atoms of a crystal surface are considered as scattering elements each having the scattering properties of a free atom. Figure 14(a) illustrates the polar diagram and total elastic cross section of a free atom; the numerical values will be explained later. When these atoms are assembled into a 2-dimensional array spaced as in the first layer of the crystal surface [Fig. 14(b)], the resulting scattering pattern will be that of a single atom multiplied by an interference function[33] which for normal incidence reduces to:

$$I_{\theta'\phi}=I_{\theta'}\frac{\sin^2 N\gamma_1}{\sin^2\gamma_1}\frac{\sin^2 M\gamma_2}{\sin^2\gamma_2}, \tag{3}$$

N and M are the number of scattering atoms along the x and y axes of the array, ϕ is the azimuthal angle measured from the positive y axis, and θ' is the scattering angle from the direction of incidence.

$\gamma_1=(2\pi/\lambda)x$, $\sin\theta'\sin\phi$;

x is the atomic spacing on the x axis,

$\gamma_2=(2\pi/\lambda)y$, $\sin\theta'\cos\phi$;

y is the atomic spacing on the y axis.

For large N, M, and for $\lambda\geq x$, or y, Eq. (3) has important values only for $\theta'=0°$ and $\theta'=180°$. The condition on λ represents energies below which all off-axis diffraction maxima are no longer observed.

The reflection coefficient for the 2-dimensional array is

$$R^*=I_{180°}/(I_{0°}+I_{180°}). \tag{4}$$

This ratio is numerically the same as for a single atom and may be obtained either from calculation or from electron scattering data. Figure 14(b) illustrates that the elastic scattering cross sections of the surface atoms cover virtually the whole surface, thus preventing simple interaction of the incident electrons with second layer atoms. Further, the surface layer atoms scatter predominantly forward and backward, suggesting that the major interfering planes might be identical rather than adjacent. This change of the main interference distance from d to D in Fig. 14(b) causes a major change in the fine structure to be expected in the reflection coefficient at low incident energies.

Electron-scattering data for tungsten vapor are unavailable, and rather than construct a theoretical potential for the tungsten atom we have used experimental data for mercury vapor. The potentials for the two atoms are nearly identical in the important range of radius $0.1\text{ Å}<r<1.5\text{ Å}$. Values of $I_{0°}$ and $I_{180°}$ for substitution into Eq. (4) were obtained by extrapolation of Arnott's data for mercury vapor,[34] which extended from 20° to 174°. For this purpose Arnott's data for energies from 4–82 eV were matched with the standard phase-shift formula given by Massey and Burhop.[32] Total cross sections were calculated from the same data by integration over all angles of scatter.

The electron on entering the solid gains kinetic energy and hence the kinetic energies of the vapor data must be reduced by an amount equivalent to the inner potential of the solid. In keeping with the atomic nature of the model the binding energy of W in the solid form, 9 eV, has been used for this correction. The reflection coefficient R^* of Eq. (4) is too large since inelastic scattering is greater in the solid than in the vapor. To account for this R^* has been multiplied by R_{exp}/δ_{exp}, where R_{exp} and δ_{exp} are the observed elastic and total reflection coefficients (see Sec. IV.1). The result of these calculations of $r=R^*R_{exp}/\delta_{exp}$ are shown in Fig. 15, where it may be seen that the model generates the

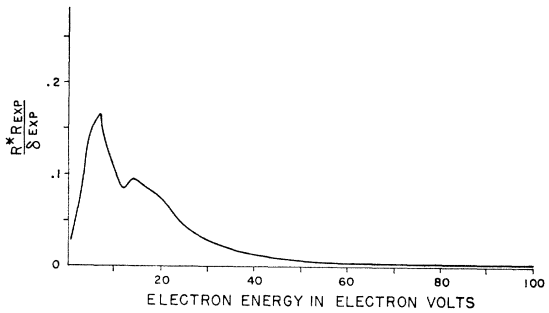

FIG. 15. Plot of $r=R^*R_{exp}/\delta_{exp}$ vs incident electron energy for tungsten (112).

[30] L. J. Schiff, *Quantum Mechanics* (McGraw-Hill Book Company, Inc., New York, 1949), p. 272.

[31] V. Bush and S. H. Caldwell, Phys. Rev. **38**, 1898 (1931).

[32] H. S. W. Massey and E. H. S. Burhop, *Electronic and Ionic Impact Phenomena* (Clarendon Press, Oxford, 1952).

[33] Z. G. Pinsker, *Electron Diffraction* (Butterworths Scientific Publications, Ltd., London, 1953), Chap. 2.

[34] F. L. Arnot, Proc. Roy. Soc. (London) **A140**, 334 (1933).

form and approximate magnitude of result (1) of Sec. IV.1.

Interference effects were calculated using the relation

$$R=|r+r(1-r)^2e^{-i2kD}|, \quad (5)$$

where D is the spacing between identical layers (see above) $k=2\pi/\lambda$. For the (100) and (110) faces D is twice the interlayer spacing and for the (112) face D is six times the interlayer spacing. The localization of the interference to the surface layers is indicated by the suppression of the fine structure in the reflection coefficient by a single layer of adsorbed gas. The values of R calculated from Eq. (5) are shown in Fig. 16 and compared with experiment. The agreement between the atomic model and experiment is seen to be better than for the one-dimensional model of Fig. 13. The fit is fairly good both in magnitude and in the width of the maxima and is qualitatively satisfactory for the locations of the main maxima. If three reflecting layers had been used the fit would not be quite as good.

Near zero energy the inelastic reflection has been found to be very small; furthermore, electrons excited photoelectrically have been found[35] to have a long mean free path. Consequently, inelastic effects may not be the mechanism which limits scattering to the first few layers at low energies. The limitation in depth may be due to the lack of longitudinal coherence in the electron beam.

With regard to the space grating a new result of the atomic model is the suggestion that identical layers of atoms may interfere more strongly in this energy range than adjacent layers. This will influence the fine structure to be expected in the off-axis diffraction maxima. However, since the experimental resolution of the diffraction measurements was not sufficient to test this conclusion, it will not be discussed further.

VI. CONCLUSIONS

(1) The major features of the elastic reflection coefficient of slow electrons incident normally on clean single crystals of tungsten (112), (100), and (110) are associated with the 0-0 diffraction beam.

(2) A model based on superposition of atomic scattering gives results closer to experimental observation than a model based on one-dimensional potential variation normal to the crystal surface.

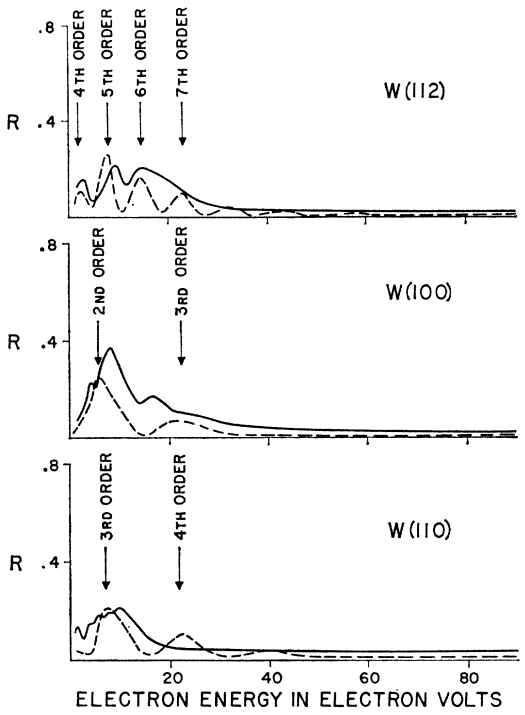

FIG. 16. Comparison between experimental results and prediction of the atomic model for reflection of slow electrons from three faces of tungsten. Solid lines: experiment; dashed lines: present model.

ACKNOWLEDGMENTS

In this work we received the assistance of many. We wish to express our sincere thanks to A. Calverley, Services Electronic Research Laboratory, Baldock, Herts., England, who supplied us with the original tungsten crystal. We are indebted to the Analytical Section of the Division of Applied Chemistry of these laboratories for the chemical analysis of the tungsten crystals. A. W. Pye, our glassblower, R. D. Cottee, and J. O. Weeks assembled the tube. Dr. P. Sewell and Dr. M. Cohen of the Division of Applied Chemistry assisted us in target preparation. We have held frequent discussions with our colleagues P. A. Redhead, E. V. Kornelsen, and A. Szabo.

[35] C. R. Crowell, W. G. Spitzer, L. E. Howarth, and E. E. Labate, Phys. Rev. **127**, 2006 (1962).

FIG. 11. Photograph of front face of tube in mirror showing diffraction pattern from tungsten (112) at 56 eV. Upper spot is 10 reflection ($\phi=90°$); side spots are 01 reflection ($\phi=0°$) and $0\bar{1}$ reflection ($\phi=180°$).